

Lattice-induced rapid formation of spin singlets in spin-1 spinor condensates

L. Zhao, T. Tang, Z. Chen, and Y. Liu*

Department of Physics, Oklahoma State University, Stillwater, Oklahoma 74078, USA

(Dated: January 3, 2018)

We experimentally demonstrate that combining a cubic optical lattice with a spinor Bose-Einstein condensate substantially relaxes three strict constraints and brings spin singlets of ultracold spin-1 atoms into experimentally accessible regions. About 80 percent of atoms in the lattice-confined spin-1 spinor condensate are found to form spin singlets, immediately after the atoms cross first-order superfluid to Mott-insulator phase transitions in a microwave dressing field. A phenomenological model is also introduced to well describe our observations without adjustable parameters.

PACS numbers: 67.85.Fg, 03.75.Kk, 03.75.Mn, 05.30.Rt

Many-body spin singlet states, in which multiple spin components of zero total spin are naturally entangled, have been widely suggested as ideal candidates in investigating quantum metrology and quantum memories [1–14]. Advantages of spin singlets in the quantum information research include long lifetimes and enhanced tolerance to environmental noises [2, 3]. These advantages may become more pronounced if the singlets consist of ultracold spin-1 particles [1]. A spin singlet is the ground state of many types of spinor gases, however, its experimental realizations have proven to be very challenging mainly due to its fragilities [3, 10, 12–15]. Allowed parameter ranges for spin singlets of spin-1 atoms are strictly limited to the vicinity of zero quadratic Zeeman energy q and zero magnetization m , and the ranges drastically shrink when the atom number increases [10–13]. Another constraint is the formation of spin singlets requires atoms remaining adiabatic for a long time duration [13, 16]. In this Letter, we experimentally demonstrate that combining a spinor Bose-Einstein condensate (BEC) with cubic optical lattices significantly relaxes these strict constraints and enables creating spin singlets of spin-1 atoms rapidly. Our observations confirm that spin singlets are brought into experimentally accessible regions by two key lattice-modified parameters, which are the lattice-enhanced interatomic interactions and substantially reduced atom number in individual lattice sites. Lattice-confined spinor BECs present degeneracies in spin and spatial domains, which provide perfect platforms to simulate quantum mesoscopic systems and study rich physics of fragmentation [7, 12].

Different methods have been proposed for detecting spin singlets. The first approach is to measure the population of each spin component, as atoms in a spin singlet should be evenly distributed into all spin states [17, 18]. The second method is to verify a spin singlet is invariant after its spin is rotated by a resonant Rf-pulse [2, 9, 12, 18, 19]. Another signature of a spin singlet is its high level of spin squeezing shown in quantum non-demolition measurements [2, 4–6]. A spin singlet can also be identified by its high-order correlation functions, e.g., its zero spin nematicity detected by light scattering

measurements [12, 20]. Other detectable parameters of a spin singlet include large population fluctuations in each of its spin components, and its excitation spectra mapped by Bragg scattering [10, 17]. In this paper, we apply the first two methods to demonstrate that about 80% of spin-1 atoms in a lattice-confined spinor BEC can form spin singlets, immediately after the atoms cross first-order superfluid (SF) to Mott-insulator (MI) phase transitions in a microwave dressing field. A phenomenological model is also developed to explain our observations without adjustable parameters.

We start each experimental cycle with an antiferromagnetic $F=1$ spinor BEC of $n = 1.2 \times 10^5$ sodium atoms and zero m in its free-space ground state, i.e., a longitudinal polar (LP) state in the $q > 0$ region or a transverse polar (TP) state when $q < 0$ [21–25]. The atoms are then loaded into cubic lattices and enter into the MI phase with the peak occupation number per lattice site being five, $n_{\text{peak}} = 5$. We express the Hamiltonian of the spinor Mott insulators by ignoring the hopping energy in the site-independent Bose-Hubbard model as [21]:

$$\hat{H} = \frac{U_0}{2}(\hat{n}^2 - \hat{n}) - \mu\hat{n} + \frac{U_2}{2}(\hat{\mathbf{S}}^2 - 2\hat{n}) + q(\hat{n}_1 + \hat{n}_{-1}). \quad (1)$$

Here U_0 (U_2) is the spin-independent (spin-dependent) interaction, μ is the chemical potential, $\hat{\mathbf{S}}$ is the spin operator, and $\hat{n} = \sum_{m_F} \hat{n}_{m_F}$ is the number operator of all hyperfine m_F states. We obtain the ground states of spinor Mott insulators by diagonalizing Eq. (1) at a given n . For example, the ground states are spin singlets at zero q in the even Mott lobes.

Sufficiently deep cubic lattices localize atoms and lower n by five orders of magnitude in a typical BEC system. Figure 1 illustrates how this enormous reduction in n together with the lattice-enhanced interatomic interactions can make spin singlets realizable in experimentally accessible regions. Figure 1 is derived from the mean-field theory (MFT) and based on two notable signatures of a spin singlet, i.e., each of its m_F states has an identical fractional population ρ_{m_F} and a big $\Delta\rho_{m_F}$ (the standard deviation of ρ_{m_F}) [10, 17, 18]. For example,

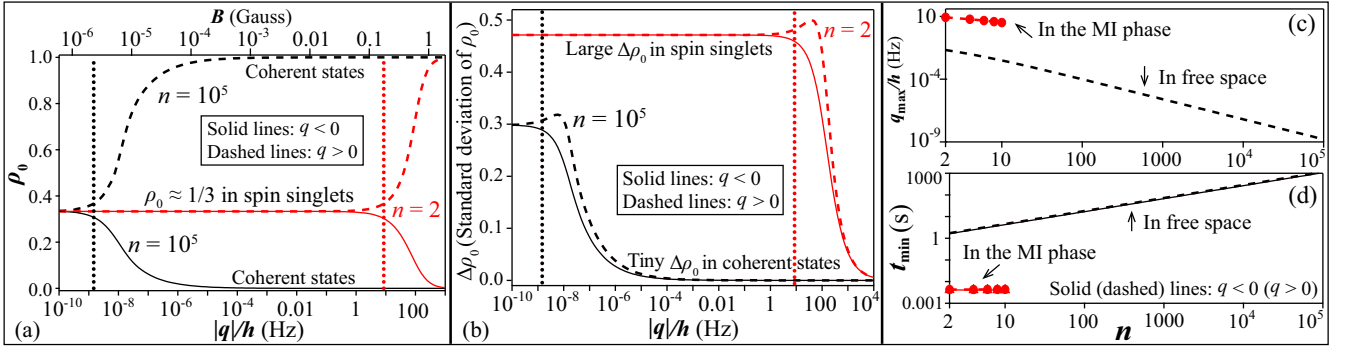


FIG. 1. (a) and (b): vertical black (red) dotted lines mark q_{\max} , the maximum allowed q for spin singlets, in $F=1$ sodium spinor BECs of $n = 10^5$ atoms in free space (in the $n=2$ Mott lobe at $u_L = 26E_R$). All panels are derived from MFT at zero m with solid (dashed) lines representing the $q < 0$ ($q > 0$) region, and black (red) lines representing spinor gases in free space (spinor Mott insulators) [16]. (a) Predicted ρ_0 versus $|q|$ at $n = 2$ (red) and 10^5 (black). The top horizontal axis lists the corresponding B when $q > 0$. (b) Predicted $\Delta\rho_0$ versus $|q|$ at $n = 2$ (red) and 10^5 (black). (c) Predicted q_{\max} versus n . (d) The minimum time t_{\min} versus n for generating singlets of sodium atoms via an adiabatic sweep at its corresponding $\pm q_{\max}$.

spin singlets of $F=1$ atoms should have $\rho_0 \approx \rho_{\pm 1} \approx 1/3$ and $\Delta\rho_0 = 2\Delta\rho_{\pm 1} > 0.29$. In sharp contrast, $\rho_0 = 0$ and $\rho_{\pm 1} = 0.5$ ($\rho_0 = 1$ and $\rho_{\pm 1} = 0$) with negligible $\Delta\rho_{m_F}$ are found in coherent TP (LP) states when $q < 0$ ($q > 0$) [24]. The allowed q range for spin singlets is $0 \leq |q| \leq q_{\max}$, which is determined by considering $\Delta\rho_{m_F} \gg 0$ and $\rho_0 = (1+0.1)/3$ at $q = q_{\max}$ (that corresponds to $\rho_0 \simeq (1-0.1)/3$ at $q = -q_{\max}$) in MFT [26]. An expansion of ten orders of magnitude in q_{\max} is marked by vertical dotted lines in Figs. 1(a) and 1(b), i.e., from a narrow region of $|q|/h < 2 \times 10^{-9}$ Hz in a free-space spinor BEC of 10^5 atoms to a much broader range of $|q|/h < 9$ Hz in $n=2$ spinor Mott insulators. Here h is the Planck constant. This drastic raise in q_{\max} as n decreases is also shown in Fig. 1(c) for a wide range of achievable n . In addition, the lattice-induced big reduction in n can relax the magnetization constraint on creating spin singlets by five orders of magnitude, because $|m| \lesssim 0.15/n$ is required for singlets at zero q [27]. Figure 1(d) indicates another big improvement made by cubic lattices: t_{\min} can be dramatically decreased by three orders of magnitude after a free-space spinor BEC enters the MI phase [16]. Here t_{\min} is the minimum time for generating singlets via adiabatically sweeping one parameter, such as q and the lattice depth u_L . Spin singlets of $F=1$ atoms can thus be created in realistic experimental setups, e.g., in the spinor Mott insulators of $|m| \leq 0.05$ as confirmed by our experimental data in Figs. 3 and 4.

In each experimental cycle, we prepare a LP or TP state at $q/h = 40$ Hz by pumping all atoms in the undesired m_F states of a $F=1$ spinor BEC to the $F=2$ state with resonant microwave pulses, and blasting away these $F=2$ atoms via a resonant laser pulse. We then quench q to a proper value in microwave dressing fields [28], and load atoms into a cubic lattice constructed by three standing waves along orthogonal directions. The lattice spacing is 532 nm, while lattice beams are originated from

a single-mode laser at 1064 nm and frequency-shifted by 20 MHz with respect to each other. We use Kapitza-Dirac diffraction patterns to calibrate u_L . Each data point in this paper is collected after atoms being abruptly released from a lattice at a fixed u_L and expanding ballistically within a given time of flight t_{TOF} . The standard Stern-Gerlach absorption imaging is a good method to measure ρ_{m_F} of spinor gases in the SF phase. Stern-Gerlach separations become indiscernible, when atoms completely lose phase coherence in the MI phase and the signal-to-noise ratio diminishes in TOF images. To measure ρ_0 in spinor Mott insulators, we develop a two-step microwave imaging method as follows: 1) count the $m_F=0$ atoms with the first imaging pulse preceded by transferring all atoms in the $|F=1, m_F=0\rangle$ state to the $F=2$ state; 2) count all remaining atoms that are in the $m_F = \pm 1$ states with the second imaging pulse. We compare these two imaging methods using a free-space spinor BEC, and find they give similar ρ_0 with a negligible difference (unless specified, all quoted uncertainties are 2 standard errors).

To ensure atoms adiabatically enter the MI phase, a cubic lattice is linearly ramped up within time t_{ramp} to $u_L = 26E_R$. Here E_R is the recoil energy [23]. We carefully select t_{ramp} based on three criteria. First, t_{ramp} should be long enough to satisfy $du_L/dt \ll 32\pi E_R^2/h$, the interband adiabaticity requirement [29]. Second, t_{ramp} should be larger than the MFT predicted t_{\min} , as explained in Fig. 1(d). These two criteria set $t_{\text{ramp}} > 5$ ms for our system. On the other hand, t_{ramp} should be sufficiently short, with $t_{\text{ramp}} \leq t_0$ to ensure lattice-induced heating is negligible and atom losses are not greater than 10%. Figure 2 explains how we determine t_0 from the observed relationship between t_{ramp} and ρ_0 in spinor Mott insulators at $u_L = 26E_R$ and $q/h = 460$ Hz. In such a high field, SF-MI phase transitions are second order because $U_2 = 0.04U_0 > 0$ and $q \gg U_2$ at this u_L for the

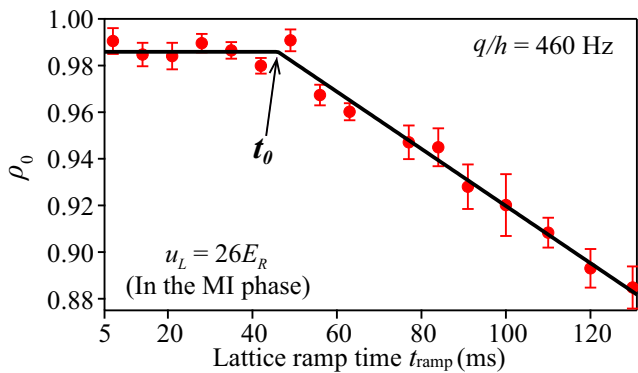


FIG. 2. Measured ρ_0 versus t_{ramp} after an initial LP spinor BEC enters the MI phase in a high field. Black lines are two linear fits. We estimate t_0 , the ideal t_{ramp} , from the intersection point of these two lines (see text).

sodium atoms [21]. Atoms initially in a LP state should thus stay in the LP state with $\rho_0 \simeq 1$, as they adiabatically cross the phase transitions and enter into the MI phase [21]. The value of ρ_0 quickly drops when inevitable heating is induced by lattices in a non-adiabatic lattice ramp sequence. We extract t_0 from the intersection point of two linear fits to the data in Fig. 2, which yields $t_{\text{ramp}} \leq t_0 \approx 45$ ms. Within this acceptable t_{ramp} range, a slower lattice ramp is preferred because it could more easily keep the system adiabatic and provide sufficient time for the atom redistribution processes [30]. The ideal lattice ramp speed is therefore set at $du_L/dt = 26E_R/t_0$ for our system.

The opposite limit is $|q| \ll U_2$ near zero q , where SF-MI phase transitions are first order and spin singlets are the ground state of $F=1$ spinor gases in the even Mott lobes [21]. We may thus identify the formation of spin singlets from evolutions of ρ_0 and $\Delta\rho_0$ during a first-order SF-MI transition. Figure 3 shows two such evolutions when atoms initially in the TP state are adiabatically loaded into the cubic lattice at the ideal lattice ramp speed to various final u_L in $q/h = -4$ Hz. These evolutions have three distinct regions. In the SF phase where $0 \leq u_L \leq 15E_R$, atoms remain in the TP state with $\rho_0 = 0$ and negligible $\Delta\rho_0$. As atoms cross first-order SF-MI transitions in $15E_R \leq u_L \leq 18E_R$, ρ_0 and $\Delta\rho_0$ sigmoidally increase with u_L . When all atoms enter into the MI phase at $u_L \geq 21E_R$, both ρ_0 and $\Delta\rho_0$ reach their equilibrium values of $\rho_0 \approx 0.3$ and $\Delta\rho_0 \gg 0$. These observations qualitatively agree with the characteristics of spin singlets. Despite that other factors can also increase $\Delta\rho_0$ in the MI phase, the measured $\Delta\rho_0$ is much smaller than the MFT prediction shown in Fig. 1(b). This may be due to the fact that the observed $\Delta\rho_0$ is an average over all 5×10^4 lattice sites in our system. Unless one can detect single lattice site precisely, the value of $\Delta\rho_0$ may not be used to verify spin singlets in lattice-confined spinor gases. We also monitor the time evolu-

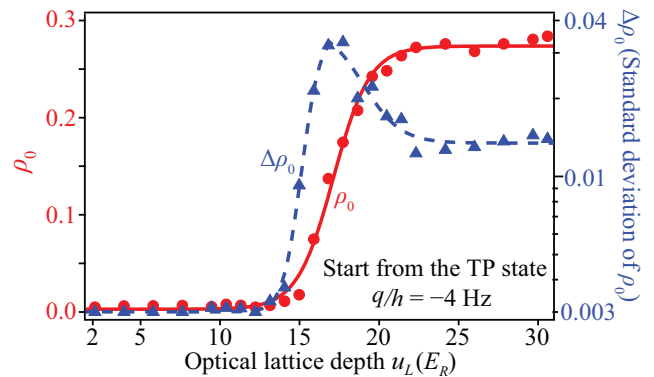


FIG. 3. Measured ρ_0 (red circles) and $\Delta\rho_0$ (blue triangles) versus u_L after an initial TP spinor BEC undergoes the ideal lattice sequence to various final u_L in a weak field near zero q . The solid line is a sigmoidal fit, and the dashed line is to guide the eye.

tion of atoms at fixed u_L and q after the ideal lattice ramp sequence. No spin oscillations are found at each q studied in this paper, which confirms atoms always stay at their ground states in these ideal lattice sequences.

We observe similar ρ_0 and $\Delta\rho_0$ evolutions within a wide range of q near zero field. The measured ρ_0 versus q in spinor Mott insulators at $u_L = 26E_R$ is shown in Fig. 4(a). These Mott insulators of $n_{\text{peak}} = 5$ are inhomogeneous systems, in which ρ_0 at a fixed q may be given by the weighted average over all Mott lobes:

$$\rho_0 = \sum_{j=1}^5 \rho_{0j} \chi_j. \quad (2)$$

Here ρ_{0j} is the MFT predicted ρ_0 in the ground state ψ_j of the $n=j$ Mott lobe, and χ_j represents mean-field atom density distributions in a harmonic trap [21]. The prediction of Eq. (2) shown by red dashed lines in Fig. 4(a), however, appears to largely disagree with our data. To understand this big discrepancy, we have tried several models and found only one phenomenological model can surprisingly describe our data without adjustable parameters (see black solid lines in Fig. 4(a)). This phenomenological model is based on one major difference between spinor and scalar Mott insulators predicted by the Bose-Hubbard model: i.e., the formation of spin singlets enlarges even Mott lobes in antiferromagnetic spinor gases [21]. For example, the $n=2$ even Mott lobe emerges at $u_L \approx 16.5E_R$, while the $n=3$ odd Mott lobe only exists in a much deeper lattice of $u_L \geq 19.5E_R$ for $F=1$ sodium spinor gases near zero field [21]. In the intermediate lattice depth of $16.5E_R < u_L < 19.5E_R$ near zero q , atoms in the $n=3$ lattice sites can freely tunnel among adjacent lattice sites, while particles in an $n=2$ lattice site already enter into the MI phase and are localized in this site. At a proper u_L near zero q , atoms may thus be able to redistribute among lattice sites with a given

odd n in the lattice-confined spinor gases. For example, at $u_L = 19E_R > 16.5E_R$, the tunneling of one atom converts two adjacent $n=3$ lattice sites to one $n=2$ and one $n=4$ sites. This u_L is then deep enough to localize the six atoms by forming a two-body spin singlet in one site and a 4-body spin singlet in the other site [30]. As a result of similar redistribution processes, atoms initially in lattice sites with $n = 5$ may form 4-body and 6-body spin singlets in the ideal lattice ramp sequences. In contrast, redistribution processes may not occur among the $n=1$ lattice sites, because the $n=1$ and $n=2$ Mott lobes emerge at similar u_L for the sodium atoms. Our phenomenological model takes these atom redistribution processes into account, and expresses ρ_0 in the spinor Mott insulators created by the ideal lattice ramp sequence as

$$\rho_0 = \sum_{j=3,5} \chi_j \frac{(j+1)\rho_{0j+1} + (j-1)\rho_{0j-1}}{2j} + \sum_{j=1,2,4} \rho_{0j} \chi_j. \quad (3)$$

Figure 4(a) shows that the prediction of Eq. (3) agrees with our experimental data. The validity of this phenomenological model is also verified by comparing its prediction with the observed ρ_0 , after a resonant Rf-pulse is applied to rotate the spin of atoms by 90 degrees. In this paper, the spin rotation operator $\hat{R}_x = \exp(-i\frac{\pi}{2}\hat{S}_x)$ is along the x -axis, which is orthogonal to the quantization axis (z -axis). After $\pi/2$ spin rotations, ρ_{0j} in Eq. (3) changes to $\rho_{0j}^r = \frac{\langle \psi_j | \hat{R}_x^\dagger \hat{n}_0 \hat{R}_x | \psi_j \rangle}{\langle \psi_j | \hat{R}_x^\dagger \hat{n} \hat{R}_x | \psi_j \rangle}$ in the $n=j$ Mott lobe. The prediction of Eq. (3) after these spin rotations is shown by the upper black solid line in Fig. 4(a), which well agrees with our data. The two data sets in Fig. 4(a) respectively represent projections of the atomic spin along two orthogonal axes. The observed good agreements between our phenomenological model and these data sets, therefore, suggest this model may reveal mechanisms of the ideal lattice ramp sequence in antiferromagnetic spinor gases.

Our data taken with and without the $\pi/2$ spin rotations appear to converge to a value around $\rho_0 \approx 1/3$ as q gets closer to zero in Fig. 4(a). This indicates the spinor Mott insulators become more rotationally invariant near zero field. As the spin rotational invariance is one unique signature of spin singlets, the reduced gap between the two data sets in Fig. 4(a) implies significant amounts of atoms may form spin singlets when q approaches zero. In our system, about 10% of atoms stay in the $n=1$ Mott lobe where no spin singlet can be formed. This accounts for the observed small gap between the two data sets near zero q in Fig. 4(a), and limits the maximum f_{ss} realizable in our system to about 90%. Here f_{ss} represents the fraction of atoms forming spin singlets in spinor gases. We extract f_{ss} from the measured ρ_0 based on Ref. [31]. The two data sets in Fig. 4(a) appear to yield similar

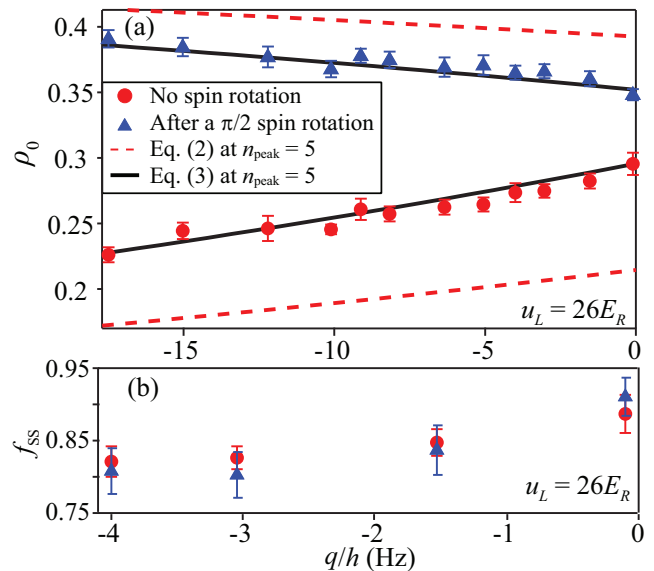


FIG. 4. (a) Red circles (blue triangles) are the measured ρ_0 in spinor Mott insulators without (with) atoms being rotated by resonant $\pi/2$ pulses at various q . The black solid (red dashed) line is the prediction of Eq. (3) (Eq. (2)). (b) Spin singlet fraction f_{ss} extracted from Panel (a) versus q (see text). The insulators are created after an initial TP spinor BEC undergoes the ideal lattice ramp sequence.

f_{ss} at a fixed q near zero field: i.e., $f_{ss} \approx 80\%$ when $-4 \text{ Hz} \leq q/h \leq 0 \text{ Hz}$ as shown in Fig. 4(b). This indicates around 80% of atoms form spin singlets in our system. Similar phenomena and slightly smaller f_{ss} are also observed in spinor Mott insulators generated after atoms initially in the LP state cross first-order SF-MI transitions in the ideal lattice ramp sequences when $q > 0$.

In conclusion, our experimental data have confirmed that combining cubic lattices with spinor BECs makes spin singlets of ultracold spin-1 atoms achievable in experimentally accessible regions. Via two independent detection methods, we have demonstrated that about 80% of atoms in the lattice-confined $F=1$ spinor BEC form spin singlets, after the atoms cross first-order SF-MI phase transitions near zero field. We have developed a phenomenological model that explains our observations without adjustable parameters. Our recent work has also indicated that we may be able to identify another signature of spin singlets, i.e., confirm their zero spin nematicity in light scattering measurements [32].

We thank the National Science Foundation and the Oklahoma Center for the Advancement of Science and Technology for financial support.

* Electronic address: yingmei.liu@okstate.edu

[1] C. C. Huang, M. S. Chang, and S. K. Yip, Phys. Rev. A **86**, 013403 (2012).

- [2] G. Tóth, and M. W. Mitchell, *New J. Phys.* **12**, 053007 (2010).
- [3] H. Sun, P. Xu, H. Pu, and W. Zhang, *Phys. Rev. A* **95**, 063624 (2017)
- [4] N. Behbood, F. Martin Ciurana, G. Colangelo, M. Napolitano, G. Tóth, R. J. Sewell, and M. W. Mitchell, *Phys. Rev. Lett.* **113**, 093601 (2014).
- [5] K. Eckert, L. Zawitkowski, A. Sanpera, M. Lewenstein, and E. S. Polzik, *Phys. Rev. Lett.* **98**, 100404 (2007).
- [6] G. Tóth, *Phys. Rev. A* **69**, 052327 (2004).
- [7] S. Ashhab and A. J. Leggett, *Phys. Rev. A* **68**, 063612 (2003).
- [8] F. Ciccarello, M. Paternostro, S. Bose, D. E. Browne, G. M. Palma, and M. Zarcone, *Phys. Rev. A* **82**, 030302(R) (2010).
- [9] I. Urizar-Lanz, P. Hyllus, I. L. Egusquiza, M. W. Mitchell, and G. Tóth, *Phys. Rev. A* **88**, 013626 (2013).
- [10] T. L. Ho and S. K. Yip, *Phys. Rev. Lett.* **84**, 4031 (2000).
- [11] C. K. Law, H. Pu, and N. P. Bigelow, *Phys. Rev. Lett.* **81**, 5257 (1998).
- [12] E. J. Mueller, T. L. Ho, M. Ueda, and G. Baym, *Phys. Rev. A* **74**, 033612 (2006).
- [13] A. Sala, D. L. Núñez, J. Martorell, L. De Sarlo, T. Zibold, F. Gerbier, A. Polls, and B. Juliá-Díaz, *Phys. Rev. A* **94**, 043623(2016).
- [14] L. De Sarlo, L. Shao, V. Corre, T. Zibold, D. Jacob, J. Dalibard, and F. Gerbier, *New J. Phys.* **15**, 113039 (2013).
- [15] Y. Eto, H. Ikeda, H. Suzuki, S. Hasegawa, Y. Tomiyama, S. Sekine, M. Sadgrove, and T. Hirano, *Phys. Rev. A* **88**, 031602(R)(2013)
- [16] Our MFT calculations are based on Ref. [24] with $t_{\min} = h/\Delta E$. Here ΔE is the energy gap between the ground state and the first excited state.
- [17] A. Imambekov, M. Lukin, and E. Demler, *Phys. Rev. A* **68**, 063602 (2003).
- [18] J. Javanainen, *J. Phys. B* **33**, 5493 (2000).
- [19] F. Zhou, *Int. J. Mod. Phys. B* **17**, 2643 (2003).
- [20] I. Carusotto and E. J. Mueller, *J. Phys. B* **37**, S115 (2004).
- [21] J. Jiang, L. Zhao, S.-T. Wang, Z. Chen, T. Tang, L.-M. Duan, and Y. Liu, *Phys. Rev. A* **93**, 063607 (2016), and the references therein.
- [22] D. M. Stamper-Kurn and M. Ueda, *Rev. Mod. Phys.* **85**, 1191 (2013).
- [23] L. Zhao, J. Jiang, T. Tang, M. Webb, and Y. Liu, *Phys. Rev. Lett.* **114**, 225302 (2015).
- [24] J. Jiang, L. Zhao, M. Webb, and Y. Liu, *Phys. Rev. A* **90**, 023610 (2014).
- [25] T.-L. Ho, *Phys. Rev. Lett.* **81**, 742 (1998); T. Ohmi and K. Machida, *J. Phys. Soc. Jpn.* **67**, 1822 (1998).
- [26] Our criterion for determining q_{\max} is stricter than those used in Refs. [13, 14].
- [27] We derive this magnetization constraint from Eq. 3 of Ref. [10].
- [28] L. Zhao, J. Jiang, T. Tang, M. Webb, and Y. Liu, *Phys. Rev. A* **89**, 023608 (2014).
- [29] J. K. Chin, D. E. Miller, Y. Liu, C. Stan, W. Setiawan, C. Sanner, K. Xu, and W. Ketterle, *Nature* **443**, 961 (2006).
- [30] The required time for the atom redistribution process is proportional to $(6nJ)^{-1}$ in cubic lattices. This may set $t_{\text{ramp}} \geq 35$ ms for our system.
- [31] Our phenomenological model predicts that $\rho_0 = f_{ss}/3 (= f_{ss}/3 + (1 - f_{ss})/2)$ in spinor Mott insulators created from an initial TP spinor BEC in the ideal lattice sequence without (with) $\pi/2$ spin rotations. This prediction only works near zero q and slightly underestimates f_{ss} .
- [32] T. Tang, L. Zhao, Z. Chen, and Y. Liu (unpublished).